Research Article

Nano Research
2020, 13(1): 138–144

ISSN 1998-0124 CN 11-5974/O4
https://doi.org/10.1007/s12274-019-2586-2

Spatial Raman mapping investigation of SERS performance related to localized surface plasmons

Yansheng Liu[1,2] and Feng Luo[1] (✉)

[1] IMDEA Nanoscience, Faraday 9, Ciudad Universitaria de Cantoblanco, 28049 Madrid, Spain
[2] School of Science, Universidad Autónoma de Madrid, Ciudad Universitaria de Cantoblanco, 28049 Madrid, Spain

Received: 30 October 2019 / **Revised:** 25 November 2019 / **Accepted:** 28 November 2019

ABSTRACT

In this research, it reported a novel three-dimensional (3D) metallic hybrid system by introducing single-layer graphene (SLG) between silver nanoparticles (NPs) and silver nano-discs (NDs) arrays (Ag NPs/SLG/Ag NDs). By combining the plasmonic metallic nanostructures and the unique physical/chemical properties of graphene, Ag NPs/SLG/Ag NDs hybrid substrate was fabricated, and it exhibited extremely high surface-enhanced Raman scattering (SERS) performance. By tuning the diameter of Ag NDs, the SERS performance of Ag NPs/SLG/Ag NDs hybrid substrate has been systematically studied. The detection limit for rhodamine 6g (R6G) could reach the concentrations as low as 1×10^{-12} mol/L, and the average enhancement factor (EF) of the Ag NPs/SLG/Ag NDs substrate could reach 5.65×10^{8}. These advantages indicated that the Ag NPs/SLG/Ag NDs hybrid substrate could be regarded as a candidate for organic molecules detection under extremely low concentration. Besides, spatial Raman mapping of Ag NPs/SLG/Ag NDs with 2.5 μm diameter NDs showed the larger SERE signal existed around the rim of Ag NDs which was related to the localized surface plasmons. This phenomenon was contributed by a larger electromagnetic field which was tuned by Ag NPs and the edge of Ag NDs. This mechanism also has been confirmed by the electromagnetic simulation result.

KEYWORDS

surface-enhanced Raman scattering (SERS), graphene, high performance, plasmon, mapping

1 Introduction

Raman spectroscopy as a very promising and powerful technique is widely applied in characterizing the chemical structures of materials without any damages. Due to its weak intensity, inelastic scattering process with a very low cross-section, fluorescence interference, inefficient light collection and detection, Raman spectroscopy technology was neglected by many researchers [1–6]. Surface-enhanced Raman scattering (SERS) as a promising method make Raman spectroscopy be a powerful technique in detecting extremely low concentration compounds [7–9], and it has exhibited amazing potential for ultrasensitive analytical applications [10–12]. Until now, SERS has been known as the only method capable of simultaneously detecting a single molecule and providing its chemical fingerprint [1, 13–16]. The widely acceptable mechanisms of SERS are chemical mechanism (CM) and electromagnetic mechanism (EM) [1, 13]. The charge transfer process between target molecules and substrate contributes to the CM mechanism [14]. EM mechanism is based on the local electromagnetic field caused by surface plasmon (SP) which is the coherent oscillations of conduction electrons under light illuminate condition [17–19]. In order to explore morphologies related electromagnetic field, different kinds of metallic structures in nanoscale with various morphologies have been explored, such as spheres [20], stars [21], cubes [22], octahedrons [23], wires [24] and pyramids [25, 26]. Among these structures, most of "hot spots" randomly generated. The disordered structures could result in unstable and un-reproducible SERS signals. Sometimes the SERS signals in random locations may be completely different. In order to avoid such disadvantages, the periodic structures have been regarded as a class of promising SERS substrates with uniformity, signal reliability, and reproducibility [27, 28]. Until now, lots of such efforts have been made in the SERS community. The researchers used different fabrication methods to synthesis controllable, periodic and reproducible structures, such as periodic nano-discs (NDs) [1, 29], nano-holes (NHs) [30, 31], nano-pillar [32], Ag nanoparticles (NPs) array [33] and Au nano-pyramid [26, 34]. These architectures were two-dimensional (2D) structures. Although the periodic 2D structures could solve the problems above mentioned in SERS, it still faced two imperfections which were 2D structures that did not fully utilize the vertical spaces, and the only gaps between horizontal patterns mainly contributed to the electromagnetic field. As a consequence, the SERS sensitivity of such simple periodic 2D structures was usually restricted by the limited density of the hot spots and the electromagnetic field [35, 36]. Due to such limits of 2D structures, the three-dimensional (3D) structures were an alternative option of making full use of vertical dimension to improve the SERS sensitivity. By fabricating "hot spots" in perpendicular dimension, electromagnetic field in the vertical gaps could also result in improving the SERS sensitivity. 3D metallic nanostructures, such as Au NPs deposited on Ag NPs [37], Au NPs decorated porous Al membrane [38], Au nanorods coupled with Ag NPs [39] and Ag nanoclusters on ZnO nano-dome arrays [40] have already been studied. For random 3D metallic nanostructures, they faced the disadvantages

Address correspondence to feng.luo@imdea.org

of the stability of SERS signals. For the periodic 3D metallic nanostructures, it remained arduous to fabricate the uniform nanometer or sub-nanometer scale structure and space.

Normally, Au and Ag are wildly applied in SERS structures. In comparison with Au, Ag has been demonstrated to possess a larger SERS enhancement factor (EF) than Au because of its absence of inter-band absorption [37, 41, 42]. In this study, Ag NPs deposited on periodic Ag NDs structures with single-layer graphene (SLG) as an intermediate component has been designed and fabricated. The porous Si_3N_4 membranes were applied as a shadow mask to generate large area (as large as 500 μm × 500 μm square), periodic and highly-ordered Ag NDs array in a few minutes. In comparison with the aluminum anodic oxide (AAO) template method, photolithography method and electron beam lithography method, this method possessed some advantages which were the fabrication time was extremely shortened and the fabrication process can be repeated several times through the same mask. The graphene material with atomic thickness generated sub-nanometer gaps between Ag NPs and Ag NDs could result in an extremely large electromagnetic field. The π–π stacking between aromatic molecules and graphene also contributed to the Raman enhancement through the charge transfer process [14, 25]. This ordered 3D metallic Ag NPs/SLG/Ag NDs structure integrated the stronger lighter interacted plasmon structure with SLG which possessed mechanical flexibility and compatibility. By applying Ag NPs/SLG/Ag NDs in detecting R6G under low concentration, we demonstrated that the periodic 3D metallic Ag NPs/SLG/Ag NDs hybrid system could be applied as a promising SERS substrate with extremely high sensitivity, good reliability, and stability.

2 Experimental sections

2.1 Fabrications of Ag NPs/SLG/Ag NDs substrates

Holey Si_3N_4 membrane with 200 nm thickness has been used as a template that was purchased from Ted Pella, Inc. The sputtering method was applied to generate 40 nm thick Ag NDs through the holey Si_3N_4 membrane. Graphene was grown on copper foil, which was deposited by atmospheric pressure chemical vapor deposition (CVD) at 1,000 °C with methane as a carbon source. In the transfer process, graphene was spin-coated with poly(methyl methacrylate) (commercial PMMA solution with the type of A4) in order to generate a supporting film. The spin coating speed was 4,000 r/min and the spin coating time was 1 min [43]. Ammonium persulfate solution (APS) bath with a concentration of 0.1 g/mL has been applied for etching copper foil. After the PMMA/SLG film was transferred on top of the Ag NDs substrate, the acetone bath was used for removing the PMMA film. Another 10 nm thick of Ag film was deposited on top of SLG/Ag NDs by using a sputtering method. In order to generate Ag NPs, the Ag film/SLG/Ag NDs sample has been annealed through the thermal treating process under the pressure of 10^{-5} mbar. The annealing temperature was 350 °C and the time was 60 min.

2.2 Raman scattering experiments

Raman scattering experiments have been carried out by using a Raman system (Bruker SENTERRA II Raman Microscope) equipped with a 532 nm incident laser. The effective power of the laser source was 2 mW for all measurements. The exposure time was 1 s. The Raman spectroscopy system was connected to a microscope, and the laser light was coupled through an objective lens of 50×, which was used for exciting the samples as well as collecting the Raman signals. Prior to each Raman experiment, calibration of the instrument was done with the Raman signal from a silicon standard centered at 521 cm^{-1}. For molecules SERS experiments, the molecules with certain concentrations have been drop-casted on the substrate. The samples were dried in the air without any heating. The SERS measurements were performed from 16 random locations in the working area to avoid some special points. If there was no special instruction, the mentioned Raman spectra were expressed in terms of average spectra.

3 Results and discussions

3.1 Characterization of the substrates

Figure 1 illustrates a brief fabrication procedure of Ag NPs/SLG/Ag NDs structure. Firstly, the holey Si_3N_4 membrane with 200 nm thickness was applied as a template. The sputtering method was applied in generating 40 nm thick Ag NDs structures through the holes in the Si_3N_4 membrane. Afterward, graphene film was transferred on top of Ag NDs by using the wet transfer method to form the SLG/Ag NDs structure. After then, 10 nm thick Ag film was deposited on top of the SLG/Ag NDs structure, and a thermal treating method was used to synthesis Ag NPs under vacuum. A detailed description of this process was described in the experimental section.

Figures 2(a), 2(c) and 2(e) are atomic force microscope (AFM) images of Ag NDs deposited on SiO_2/Si substrate with three different diameters. They illustrated the periodic and homogenous Ag NDs structures which proved the feasibility of fabrication. The heights and diameters of the Ag NDs have been illustrated in cross-section profiles which are illustrated in Figs. S1(a), S1(c) and S1(e) in the Electronic Supplementary Material (ESM). The heights of all Ag NDs were 40 nm which was controlled by the deposition time, and the diameters of Ag NDs are 2.5 μm, 1 μm and 500 nm. The edge to edge distances of Ag NDs were the same as the NDs diameter which were 2.5 μm, 1 μm and 500 nm, respectively. From Figs. 2(b), 2(d) and 2(f), it can be observed that the morphology of Ag NDs was maintained and the Ag NDs were successfully decorated by Ag NPs in which graphene as an intercalation layer. The generation of Ag NPs owed to the spatial reactivity during the annealing process, which led to local nucleation sites and the growth of small NPs [32, 37]. The corresponding cross-section profiles are illustrated in Figs. S1(b), S1(d), and S1(f) in the ESM.

To test the SERS performance of the Ag NPs/SLG/Ag NDs with three different NDs diameters, rhodamine 6g (R6G) was applied as a probe molecule. The 20 μL of R6G ethanol solution

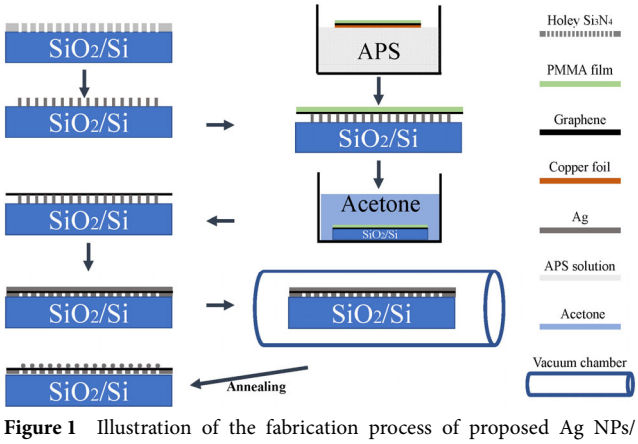

Figure 1 Illustration of the fabrication process of proposed Ag NPs/SLG/Ag NDs structure.

with a concentration of 1×10^{-6} mol/L was dispersed on the three substrates with the same total area to avoid concentration effects. The SERS spectra were averaged spectra which were obtained from 16 random locates. In Fig. 3, the Raman shifts located at 610, 772, 1,181, 1,506 and 1,647 cm^{-1} can be observed and these peaks have a good agreement with the characteristic peaks of R6G [44, 45]. By comparison with the Raman intensity of the substrate with different diameters, the 500 nm diameter Ag NDs showed the largest SERS enhancement. This was caused by the larger electromagnetic field of smaller NDs substrate [30].

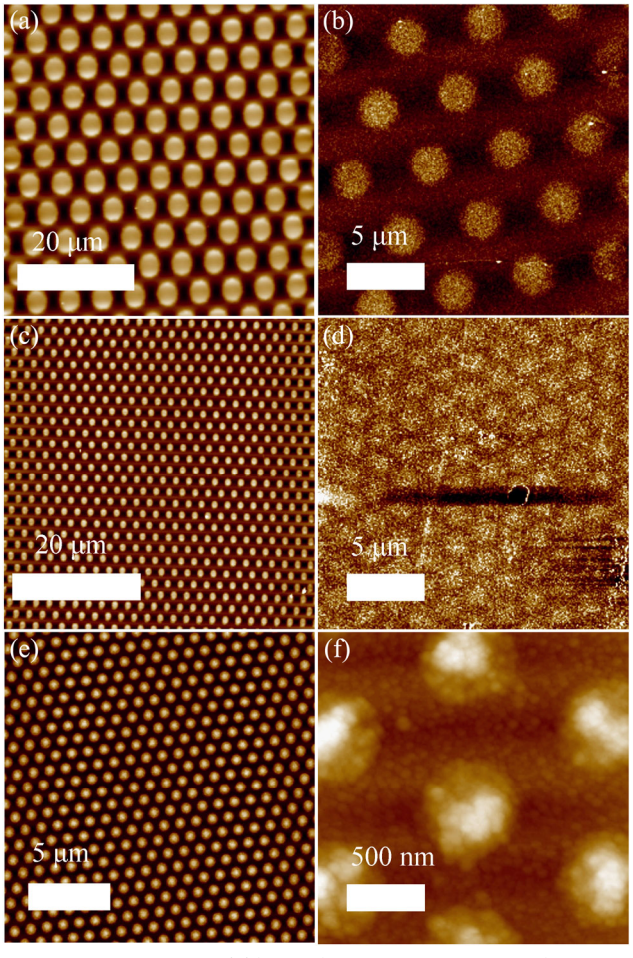

Figure 2 AFM images of fabricated Ag NDs on SiO_2/Si and Ag NPs/SLG/Ag NDs structures. (a), (c) and (e) AFM images of Ag NDs deposited on SiO_2/Si substrate with the NDs diameter of 2.5 μm, 1 μm and 500 nm, respectively. (b), (d) and (f) AFM images of Ag NPs/SLG/Ag NDs structure with the NDs diameter of 2.5 μm, 1 μm and 500 nm, respectively.

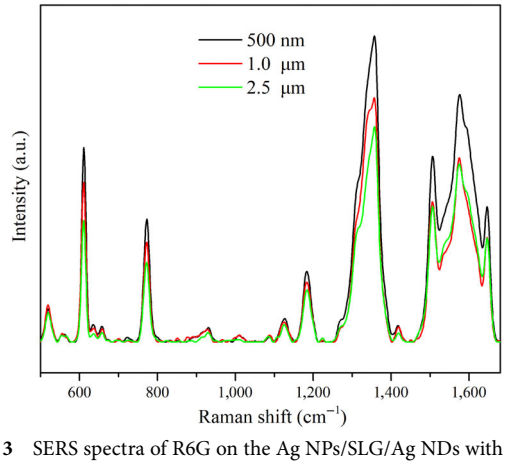

Figure 3 SERS spectra of R6G on the Ag NPs/SLG/Ag NDs with 2.5 μm, 1 μm and 500 nm diameters NDs array structures. The concentration of R6G was 1×10^{-6} mol/L.

3.2 SERS spectra of different molecule concentrations

To investigate the SERS performance and sensitivity of the proposed Ag NPs/SLG/Ag NDs, the SERS spectra of R6G with different concentrations, which were drop-casted on of Ag NPs/SLG/Ag NDs with 500 nm diameter NDs array, have been illustrated in Fig. 4(a). The SERS signals of R6G under the concentration of 1×10^{-12} mol/L can be observed which proved the superior detection limit of Ag NPs/SLG/Ag NDs substrate. This detection limit was lower than proposed reported substrates, such as single-layer graphene-Au NP with the detection limit of 1×10^{-8} mol/L [46], 1LG/Ag NP array with the detection limit of 1×10^{-11} mol/L [13], Ag NP/GO with the detection limit of 1×10^{-7} mol/L [47], Au NP/1LG/Au NP with the detection limit of 1×10^{-10} mol/L [48], Au NP/RGO/Ag dendrite with the detection limit of 1×10^{-8} mol/L [41] and Au@Ag NP/GO/Au@Ag NP with the detection limit of 1×10^{-11} mol/L [49]. With increasing the concentration of R6G molecule, the SERS signals of the above characteristic peaks were significantly improved. For the SERS spectrum with the concentration of 1×10^{-6} mol/L, the Raman shifts located at 610, 772, 1,181, 1,506 and 1,647 cm^{-1} became much clear, and these peaks showed a good agreement with previous reports [44, 45]. Under the R6G concentration of 1×10^{-6} mol/L, not only the characteristic peaks of R6G were observed, but also

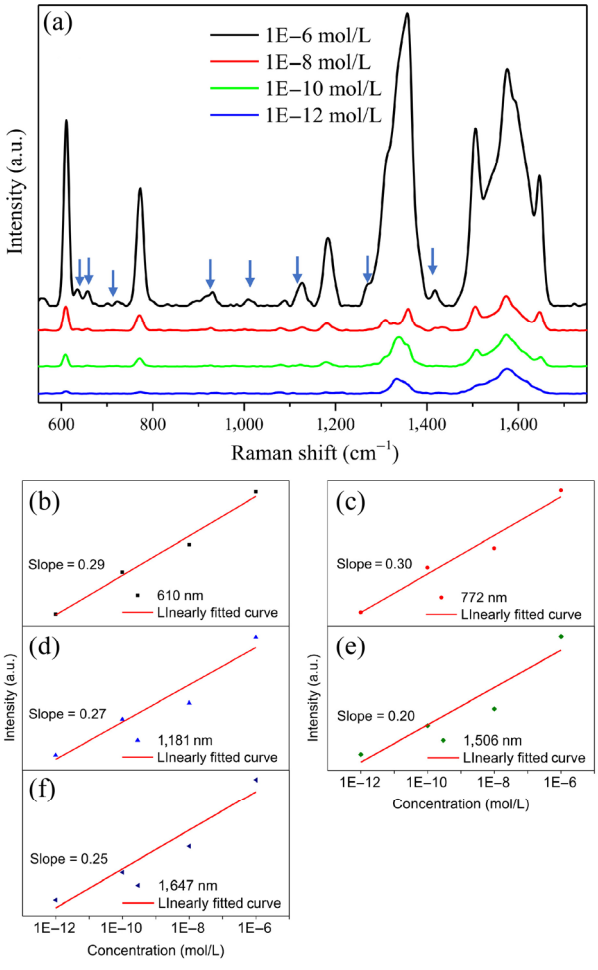

Figure 4 (a) SERS spectra of R6G on Ag NPs/SLG/Ag NDs with 500 nm diameter NDs array with the concentrations from 1×10^{-12} to 1×10^{-6} mol/L. (b)–(f) Integral peak intensities of R6G molecules as a function of concentrations. The selected Raman shifts in (b)–(f) were 610, 772, 1,181, 1,506 and 1,647 cm^{-1}, respectively.

some additional weak peaks were shown as marked by blue arrows. These additional peaks could be ascribed to chemical adsorption-induced vibrations, molecular deformation, and distortion [50, 51]. Various possible interactions between Ag NPs/SLG/Ag NDs substrate and the R6G molecules, such as charge transfer between the metal and molecules, photo-induced damage and metal-catalyzed side reactions, may all affect the final signals and make it difficult to assign these additionally peaks precisely to a SERS spectrum [2, 52]. To verify the capacity of quantitative detection, the relations between the logarithm of the SERS intensities and concentrations were illustrated in Figs. 4(b)–4(f), and the characteristic peaks located at 610, 772, 1,181, 1,506 and 1,647 cm^{-1} were selected. From the linearly fitted curves, the intensities of the SERS spectra of R6G were proportional to the logarithm of the concentrations of R6G ethanol solution. By averaging, the relation between SERS signal intensity and molecules concentration could be written as

$$\lg(I_{SERS}) = 0.26\lg(C_{SERS}) + 4.9 \quad (1)$$

Through the linear response from 1×10^{-6} to 1×10^{-12} mol/L in log scale, it revealed that the metallic Ag NPs/SLG/Ag NDs substrate possessed a great potential in identifying and quantitatively detecting organic materials.

The EF of SERS for R6G on the Ag NPs/SLG/Ag NDs substrates could be calculated through the standard equation [13, 33, 53]

$$EF = \frac{I_{SERS} / N_{SERS}}{I_{RS} / N_{RS}} \quad (2)$$

where I_{SERS} and I_{RS} correspond to peaks intensities of the SERS spectra and the normal Raman spectra, respectively. N_{SERS} and N_{RS} are the numbers of molecules absorbed on the substrates with or without "hot spots". In EF calculated experiments, R6G ethanol solution with a certain volume V_{SERS} and concentration C_{SERS} was dropped on the SERS-active substrates to get SERS signal. For non-SERS substrate, a certain volume V_{RS} of R6G ethanol solution with a concentration of C_{RS} was dispersed to an area of S_{RS} on a clean SiO_2/Si substrate, and let it dry to form R6G solid thin film. Thus Eq. (2) could be converted to

$$EF = \frac{I_{SERS}}{I_{RS}} \frac{S_{SERS} V_{RS} C_{RS}}{S_{RS} V_{SERS} C_{SERS}} \quad (3)$$

Figure 5 showed the SERS spectrum and the normal Raman spectrum of R6G from the Ag NPs/SLG/Ag NDs substrate and SiO_2/Si substrate. The peak intensities of 610 cm^{-1} have been selected to calculate the EF. For SERS spectrum, 20 μL of 1×10^{-12} mol/L R6G ethanol solution was dispersed to a total area of about 1 cm × 1 cm substrate (the working area of Ag NPs/SLG/Ag NDs was 500 μm × 500 μm), and 20 μL of 1×10^{-4} mol/L R6G solution was dispersed on SiO_2/Si substrate with a total area of about 1 cm × 1 cm. For the calculation, we considered the dried molecules film on the surface of the total substrate surface was homogeneous. Consequently, both S_{SERS} and S_{RS} were regarded as 1 cm^2. In Fig. 5, the peak intensities of solid R6G film on Ag NPs/SLG/Ag NDs and SiO_2/Si substrates were 87.5 and 17.5 counts, respectively. According to the Eq. (3), the calculated EF was 5.65×10^8 for the Ag NPs/SLG/Ag NDs array substrates. This experimental EF was the average value of the total SERS substrate. In Li's work, the simulated EF of Ag NPs-graphene-Ag substrate film was 1.02×10^9 [54]. However, this value was calculated only from the largest electromagnetic field region. The average experimental EF of G/Ag NP array substrates reported by Zhang was 4.8×10^7 [53]. For the Au NPs-SLG-Au NPs substrate in Khang June Lee's work, the

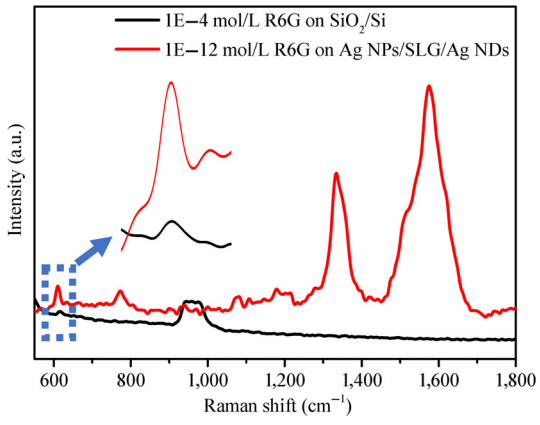

Figure 5 The SERS spectrum of R6G ethanol solution with the concentration of 1×10^{-12} mol/L which was dispersed to a total area of about 1 cm × 1 cm substrate, and normal Raman spectrum of R6G solution with the concentration of 1×10^{-4} mol/L was dispersed on SiO_2/Si with the total area of about 1 cm × 1 cm.

average experimental EF was 2.9×10^5 [55]. By comparison, it proved the excellent SERS performance of proposed Ag NPs/SLG/Ag NDs substrates.

3.3 Spatial Raman mappings of Ag NPs/SLG/Ag NDs substrates with 2.5 μm diameter NDs

Spatial Raman mappings of Ag NPs/SLG/Ag NDs substrates with 2.5 μm diameter NDs have been illustrated in Fig. 6. The scanning area was 4 μm × 4 μm, and the resolution was 10 pixels × 10 pixels with a division of 400 nm. Figure 6(a) illustrates the Spatial Raman mapping of Si. In Fig. 6(a), the Ag NDs covered area shows less Raman intensity, and the space between NDs shows stronger Raman signal. Figures 6(b)–6(d) are spatial Raman mappings at 1,340, 1,580 and 1,680 cm^{-1} which belong to D band, G band and 2D band of graphene, respectively. From Figs. 6(b)–6(d), it can be observed that the SERS signals of D band, G band and 2D band mainly enhanced at the rim of NDs. We believe this phenomenon due to the larger electromagnetic field tuned by Ag NPs which were located at the rim area of Ag NDs. Figure S2 in the ESM illustrates

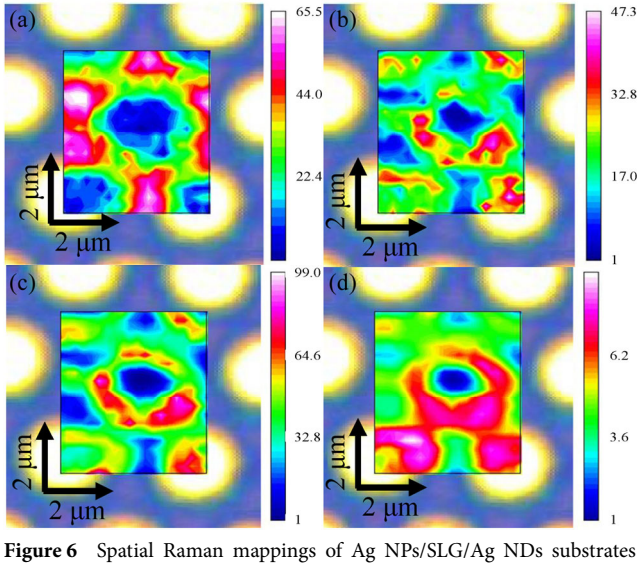

Figure 6 Spatial Raman mappings of Ag NPs/SLG/Ag NDs substrates with 2.5 μm diameter NDs. Raman intensities at 521 (a), 1,340 (b), 1,580 (c) and 1,680 cm^{-1} (d) which belonged to Si, D band, G band and 2D band of graphene, respectively. The background images were the optical image of Ag NPs/SLG/Ag NDs and the color distributions illustrated the region where was scanned.

a typical SERS spectrum of SLG from Ag NPs/SLG/Ag NDs substrates and normal SLG Raman spectrum with 532 nm incident laser. By comparison with the normal Raman spectrum, the G band of graphene has been extremely enhanced resulting in the larger EF(G) than EF(2D). This caused the SERS signal of G band larger than the 2D band [56, 57]. D band of graphene was considered as a sign of disordered graphene [58, 59]. The appearance of the D band was caused by the possibilities of the graphene break and wrinkles in the transfer process or the original defects in the graphene growing process.

3.4 Spatial Raman mappings of R6G and fluorescein drop-casted on Ag NPs/SLG/Ag NDs substrates with 2.5 μm diameter NDs

To testify the applicability Ag NP/SLG/Ag NDs substrates, R6G and fluorescein were selected as analytes. The scanning area was 8 μm × 8 μm, and the resolution was 20 pixels × 20 pixels with a division of 400 nm. Figures 7(a)–7(d) illustrate the spatial Raman mappings of R6G and fluorescein molecules drop-casted on Ag NPs/SLG/Ag NDs with 2.5 μm diameter NDs. The substrates employed in detecting R6G and fluorescein were not the same noes, and they came from different batches. Figures S3(a) and S3(b) in the ESM are typical Raman spectra obtained from R6G and fluorescein molecules drop-casted on Ag NP/SLG/Ag NDs substrate. In Fig. S3(b) in the ESM, the Raman shifts located at 595, 636, 763, 1,182, 1,331, 1,409, 1,549 and 1,634 cm^{-1} can be clearly observed. These peaks agreed with the characteristic peaks of fluorescein [60–62]. Integral Raman intensity of 521 cm^{-1} in Figs. 7(a) and 7(c) belonged to Si, and the color distributions clearly showed the circular patterns which revealed the position of Ag NDs. In Figs. 7(b) and 7(d), the integral Raman intensities of 1,182 cm^{-1} belonging to R6G and 611 cm^{-1} belonging to fluorescein have been illustrated.

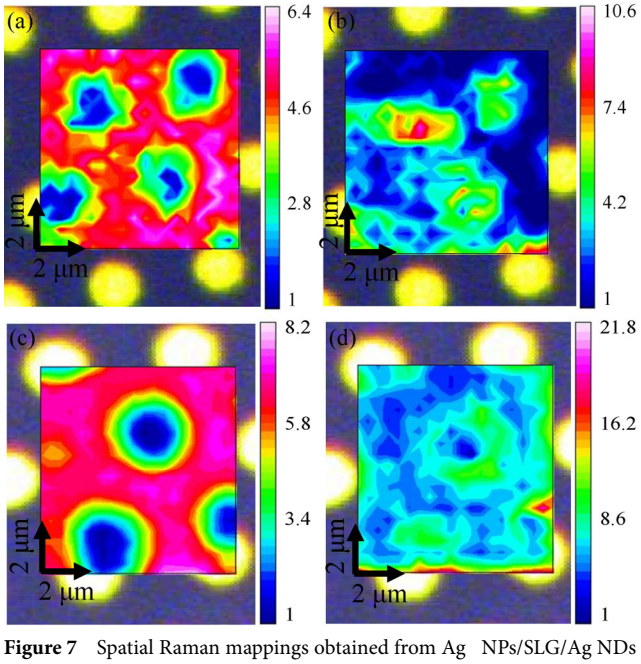

Figure 7 Spatial Raman mappings obtained from Ag NPs/SLG/Ag NDs substrates with 2.5 μm diameter NDs which was drop-casted by 20 μL of R6G solution with the concentration of 1 × 10^{-6} mol/L, and fluorescein molecules with the concentration of 1 × 10^{-4} mol/L. (a) and (c) The distribution of integral peak intensities at 521 cm^{-1} which corresponded to Si. (b) The distribution of integral peak intensity at 1,182 cm^{-1} which corresponded to fluorescein. (d) The distribution of integral peak intensity at 611 cm^{-1} which corresponded to R6G. The background images were the optical image of Ag NPs/SLG/Ag NDs and the color distributions illustrated the region where was scanned.

From the color distributions in both images, it can be observed that the larger Raman intensities mainly located around the rims of Ag NDs, and they looked like "rings". This ring structure was contributed by the larger electromagnetic field of the edge of the metallic structure [63–66]. In Ag NPs/SLG/Ag NDs structure, the edge electromagnetic field of Ag NDs has been amplified by demarcating Ag NPs with a sub-nanometer gap (carbon atom thickness). Consequentially, the SERS signal of molecules absorbed in such a rim region was extremely enhanced. This result has been proved through the simulation result in Fig. 8.

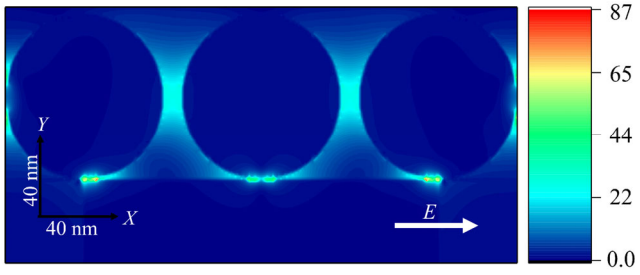

Figure 8 The simulated electromagnetic field in the *YZ* plane of simplified model.

3.5 Electromagnetic field simulation performance

To better understand the nature of the EM mechanism of SERS, the electromagnetic field simulation of Ag NPs/SLG/Ag NDs substrate has been performed. The simplified model has been applied and the simulated result was displayed in Fig. 8. In the simulation part, a plane light wave was launched perpendicular to the substrate with a wavelength of 532 nm. The *X*-, *Y*- and *Z*-axes were using perfectly matched layer (PML) boundary conditions. The structure was 40 nm thick Ag NDs array with a diameter of 180 nm. 1 nm thick graphene was applied. The circular Ag NPs with 80 nm diameter and 10 nm edge to edge distance were decorated on top of graphene. The meshing setting was 1 nm in *X*-, *Y*- and *Z*-directions. From the simulated results of the simplified model, it was clear the edge of the structure showed a large electromagnetic field which matched the result of spatial Raman mapping results.

4 Conclusions

In conclusion, this work presented an efficient strategy for designing and fabricating high-performance SERS substrates and confirmed the EM mechanism of SERS. By combining the EM of Ag NPs and Ag NDs as well as the unique properties of single graphene, Ag NPs/SLG/Ag NDs illustrated high SERS sensitivity. The SERS enhancement of Ag NPs/SLG/Ag NDs substrate has been modulated by varying the diameter of Ag NDs from 500 nm to 2.5 μm and the substrate with 500 nm Ag NDs diameter possessed large EF. By analyzing the spatial Raman mapping of Ag NPs/SLG/Ag NDs with 2.5 μm NDs diameter, the lager enhancement region was mainly at the rim of Ag NDs due to the larger electromagnetic field of this region. This has been proved through the electromagnetic field simulation results. The high performance of Ag NPs/SLG/Ag NDs indicated it could be a promising candidate in characterizing the molecules under extremely low concentration.

Acknowledgements

This work has been supported by China Scholarship Council, the National Natural Science Foundation of China (Nos. 201606180013 and 51520105003) and MINISTERIO DE

ECONOMÍA, INDUSTRIA Y COMPETITIVIDAD (No. MAT2017-89868-P).

Electronic Supplementary Material: Supplementary material (cross-section files corresponding to Fig. 2, SERS spectrum of graphene obtained from Ag NPs/SLG/Ag NDs, and the Raman spectra of R6G and fluorescein molecules on Ag NPs/SLG/Ag NDs substrate with 2.5 μm diameter Ag NDs) is available in the online version of this article at https://doi.org/10.1007/s12274-019-2586-2.

References

[1] Schedin, F.; Lidorikis, E.; Lombardo, A.; Kravets, V. G.; Geim, A. K.; Grigorenko, A. N.; Novoselov, K. S.; Ferrari, A. C. Surface-enhanced Raman spectroscopy of graphene. *ACS Nano* **2010**, *4*, 5617–5626.

[2] Xu, W. G.; Ling, X.; Xiao, J. Q.; Dresselhaus, M. S.; Kong, J.; Xu, H. X.; Liu, Z. F.; Zhang, J. Surface enhanced Raman spectroscopy on a flat graphene surface. *Proc. Natl. Acad. Sci. USA.* **2012**, *109*, 9281–9286.

[3] Reokrungruang, P.; Chatnuntawech, I.; Dharakul, T.; Bamrungsap, S. A simple paper-based surface enhanced Raman scattering (SERS) platform and magnetic separation for cancer screening. *Sens. Actuators B: Chem.* **2019**, *285*, 462–469.

[4] Mosier-Boss, P. A. Review of SERS substrates for chemical sensing. *Nanomaterials* **2017**, *7*, 142.

[5] Li, X. L.; Zhang, Y. Z.; Shen, Z. X.; Fan, H. J. Highly ordered arrays of particle-in-bowl plasmonic nanostructures for surface-enhanced Raman scattering. *Small* **2012**, *8*, 2548–2554.

[6] Li, X. L.; Hu, H. L.; Li, D. H.; Shen, Z. X.; Xiong, Q. H.; Li, S. Z.; Fan, H. J. Ordered array of gold semishells on TiO_2 spheres: An ultrasensitive and recyclable SERS substrate. *ACS Appl. Mater. Interfaces* **2012**, *4*, 2180–2185.

[7] Le Ru, E. C.; Etchegoin, P. G. Single-molecule surface-enhanced Raman spectroscopy. *Annu. Rev. Phys. Chem.* **2012**, *63*, 65–87.

[8] Willets, K. A. Super-resolution imaging of SERS hot spots. *Chem. Soc. Rev.* **2014**, *43*, 3854–3864.

[9] Ling, X.; Huang, S. X.; Deng, S. B.; Mao, N. N.; Kong, J.; Dresselhaus, M. S.; Zhang, J. Lighting up the Raman signal of molecules in the vicinity of graphene related materials. *Acc. Chem. Res.* **2015**, *48*, 1862–1870.

[10] Fleischmann, M.; Hendra, P. J.; McQuillan, A. J. Raman spectra of pyridine adsorbed at a silver electrode. *Chem. Phys. Lett.* **1974**, *26*, 163–166.

[11] Albrecht, M. G.; Creighton, J. A. Anomalously intense Raman spectra of pyridine at a silver electrode. *J. Am. Chem. Soc.* **1977**, *99*, 5215–5217.

[12] Jeanmaire, D. L.; Van Duyne, R. P. Surface Raman spectroelectrochemistry: Part I. Heterocyclic, aromatic, and aliphatic amines adsorbed on the anodized silver electrode. *J. Electroanal. Chem. Interf. Electrochem.* **1977**, *84*, 1–20.

[13] Xu, S. C.; Jiang, S. Z.; Wang, J. H.; Wei, J.; Yue, W. W.; Ma, Y. Graphene isolated Au nanoparticle arrays with high reproducibility for high-performance surface-enhanced Raman scattering. *Sens. Actuators B: Chem.* **2016**, *222*, 1175–1183.

[14] Nie, S. M.; Emory, S. R. Probing single molecules and single nanoparticles by surface-enhanced Raman scattering. *Science* **1997**, *275*, 1102–1106.

[15] Huang, X. H.; El-Sayed, I. H.; Qian, W.; El-Sayed, M. A. Cancer cell imaging and photothermal therapy in the near-infrared region by using gold nanorods. *J. Am. Chem. Soc.* **2006**, *128*, 2115–2120.

[16] Ling, X.; Xie, L. M.; Fang, Y.; Xu, H.; Zhang, H. L.; Kong, J.; Dresselhaus, M. S.; Zhang, J.; Liu, Z. F. Can graphene be used as a substrate for Raman enhancement? *Nano Lett.* **2010**, *10*, 553–561.

[17] Yang, S. K.; Dai, X. M.; Stogin, B. B.; Wong, T. S. Ultrasensitive surface-enhanced Raman scattering detection in common fluids. *Proc. Natl. Acad. Sci. USA* **2016**, *113*, 268–273.

[18] Fan, W.; Lee, Y. H.; Pedireddy, S.; Zhang, Q.; Liu, T. X.; Ling, X. Y. Graphene oxide and shape-controlled silver nanoparticle hybrids for ultrasensitive single-particle surface-enhanced Raman scattering (SERS) sensing. *Nanoscale* **2014**, *6*, 4843–4851.

[19] Zhao, Y.; Yang, D.; Li, X. Y.; Liu, Y.; Hu, X.; Zhou, D. F.; Lu, Y. L. Toward highly sensitive surface-enhanced Raman scattering: The design of a 3D hybrid system with monolayer graphene sandwiched between silver nanohole arrays and gold nanoparticles. *Nanoscale* **2017**, *9*, 1087–1096.

[20] Li, L.; Hutter, T.; Steiner, U.; Mahajan, S. Single molecule SERS and detection of biomolecules with a single gold nanoparticle on a mirror junction. *Analyst* **2013**, *138*, 4574–4578.

[21] Lee, J.; Hua, B.; Park, S.; Ha, M.; Lee, Y.; Fan, Z. Y.; Ko, H. Tailoring surface plasmons of high-density gold nanostar assemblies on metal films for surface-enhanced Raman spectroscopy. *Nanoscale* **2014**, *6*, 616–623.

[22] Rycenga, M.; Xia, X. H.; Moran, C. H.; Zhou, F.; Qin, D.; Li, Z. Y.; Xia, Y. N. Generation of hot spots with silver nanocubes for single-molecule detection by surface-enhanced Raman scattering. *Angew. Chem., Int. Ed.* **2011**, *50*, 5473–5477.

[23] Xia, X. H.; Zeng, J.; McDearmon, B.; Zheng, Y. Q.; Li, Q. G.; Xia, Y. N. Silver nanocrystals with concave surfaces and their optical and surface-enhanced Raman scattering properties. *Angew. Chem., Int. Ed.* **2011**, *50*, 12542–12546.

[24] Tao, A.; Kim, F.; Hess, C.; Goldberger, J.; He, R. R.; Sun, Y. G.; Xia, Y. N.; Yang, P. D. Langmuir−Blodgett silver nanowire monolayers for molecular sensing using surface-enhanced Raman spectroscopy. *Nano Lett.* **2003**, *3*, 1229–1233.

[25] Wang, P.; Liang, O. W.; Zhang, W.; Schroeder, T.; Xie, Y. H. Ultra-sensitive graphene-plasmonic hybrid platform for label-free detection. *Adv. Mater.* **2013**, *25*, 4918–4924.

[26] Wang, P.; Xia, M.; Liang, O. W.; Sun, K.; Cipriano, A. F.; Schroeder, T.; Liu, H. N.; Xie, Y. H. Label-free SERS selective detection of dopamine and serotonin using graphene-Au nanopyramid heterostructure. *Anal. Chem.* **2015**, *87*, 10255–10261.

[27] Palankar, R.; Medvedev, N.; Rong, A.; Delcea, M. Fabrication of quantum dot microarrays using electron beam lithography for applications in analyte sensing and cellular dynamics. *ACS Nano* **2013**, *7*, 4617–4628.

[28] Abu Hatab, N. A.; Oran, J. M.; Sepaniak, M. J. Surface-enhanced Raman spectroscopy substrates created via electron beam lithography and nanotransfer printing. *ACS Nano* **2008**, *2*, 377–385.

[29] Kravets, V. G.; Schedin, F.; Jalil, R.; Britnell, L.; Novoselov, K. S.; Grigorenko, A. N. Surface hydrogenation and optics of a graphene sheet transferred onto a plasmonic nanoarray. *J. Phys. Chem. C* **2012**, *116*, 3882–3887.

[30] Yu, Q. M.; Guan, P.; Qin, D.; Golden, G.; Wallace, P. M. Inverted size-dependence of surface-enhanced Raman scattering on gold nanohole and nanodisk arrays. *Nano Lett.* **2008**, *8*, 1923–1928.

[31] Hao, Q. Z.; Wang, B.; Bossard, J. A.; Kiraly, B.; Zeng, Y.; Chiang, I. K.; Jensen, L.; Werner, D. H.; Huang, T. J. Surface-enhanced Raman scattering study on graphene-coated metallic nanostructure substrates. *J. Phys. Chem. C* **2012**, *116*, 7249–7254.

[32] Huang, Z. L.; Meng, G. W.; Huang, Q.; Yang, Y. J.; Zhu, C. H.; Tang, C. L. Improved SERS performance from Au nanopillar arrays by abridging the pillar tip spacing by Ag sputtering. *Adv. Mater.* **2010**, *22*, 4136–4139.

[33] Mu, C.; Zhang, J. P.; Xu, D. S. Au nanoparticle arrays with tunable particle gaps by template-assisted electroless deposition for high performance surface-enhanced Raman scattering. *Nanotechnology* **2010**, *21*, 015604.

[34] Wang, P.; Zhang, W.; Liang, O. W.; Pantoja, M.; Katzer, J.; Schroeder, T.; Xie, Y. H. Giant optical response from graphene–plasmonic system. *ACS Nano* **2012**, *6*, 6244–6249.

[35] Ko, H.; Singamaneni, S.; Tsukruk, V. V. Nanostructured surfaces and assemblies as SERS media. *Small* **2008**, *4*, 1576–1599.

[36] Kodiyath, R.; Malak, S. T.; Combs, Z. A.; Koenig, T.; Mahmoud, M. A.; El-Sayed, M. A.; Tsukruk, V. V. Assemblies of silver nanocubes for highly sensitive SERS chemical vapor detection. *J. Mater. Chem. A* **2013**, *1*, 2777–2788.

[37] Zhao, Y.; Zeng, W. C.; Tao, Z. C.; Xiong, P. H.; Qu, Y.; Zhu, Y. W. Highly sensitive surface-enhanced Raman scattering based on multi-dimensional plasmonic coupling in Au-graphene-Ag hybrids. *Chem. Commun.* **2015**, *51*, 866–869.

[38] Ko, H.; Tsukruk, V. V. Nanoparticle-decorated nanocanals for surface-enhanced Raman scattering. *small* **2008**, *4*, 1980–1984.

[39] Sivashanmugan, K.; Liao, J. D.; Shao, P. L.; Haochih Liu, B.; Tseng, T. Y.; Chang, C. Y. Intense Raman scattering on hybrid Au/Ag nano-platforms for the distinction of MMP-9-digested collagen type-I fiber detection. *Biosens. Bioelectron.* **2015**, *72*, 61–70.
[40] Sivashanmugan, K.; Liao, J. D.; Liu, B. H.; Yao, C. K.; Luo, S. C. Ag nanoclusters on ZnO nanodome array as hybrid SERS-active substrate for trace detection of malachite green. *Sens. Actuators B: Chem.* **2015**, *207*, 430–436.
[41] Liu, A. P.; Xu, T.; Tang, J.; Wu, H. P.; Zhao, T. Y.; Tang, W. H. Sandwich-structured Ag/graphene/Au hybrid for surface-enhanced Raman scattering. *Electrochim. Acta* **2014**, *119*, 43–48.
[42] Han, Y.; Lupitskyy, R.; Chou, T. M.; Stafford, C. M.; Du, H.; Sukhishvili, S. Effect of oxidation on surface-enhanced Raman scattering activity of silver nanoparticles: A quantitative correlation. *Anal. Chem.* **2011**, *83*, 5873–5880.
[43] Li, X. S.; Cai, W. W.; An, J.; Kim, S.; Nah, J.; Yang, D. X.; Piner, R.; Velamakanni, A.; Jung, I.; Tutuc, E. et al. Large-area synthesis of high-quality and uniform graphene films on copper foils. *Science* **2009**, *324*, 1312–1314.
[44] Thrall, E. S.; Crowther, A. C.; Yu, Z. H.; Brus, L. E. R6G on graphene: High Raman detection sensitivity, yet decreased Raman cross-section. *Nano Lett.* **2012**, *12*, 1571–1577.
[45] Lu, R. T.; Konzelmann, A.; Xu, F.; Gong, Y. P.; Liu, J. W.; Liu, Q. F.; Xin, M.; Hui, R. Q.; Wu, J. Z. High sensitivity surface enhanced Raman spectroscopy of R6G on *in situ* fabricated Au nanoparticle/graphene plasmonic substrates. *Carbon* **2015**, *86*, 78–85.
[46] Du, Y. X.; Zhao, Y.; Qu, Y.; Chen, C. H.; Chen, C. M.; Chuang, C. H.; Zhu, Y. W. Enhanced light–matter interaction of graphene–gold nanoparticle hybrid films for high-performance SERS detection. *J. Mater. Chem. C* **2014**, *2*, 4683–4691.
[47] Liang, X.; Liang, B. L.; Pan, Z. H.; Lang, X. F.; Zhang, Y. G.; Wang, G. S.; Yin, P. G.; Guo, L. Tuning plasmonic and chemical enhancement for SERS detection on graphene-based Au hybrids. *Nanoscale* **2015**, *7*, 20188–20196.
[48] Zhao, Y.; Li, X. Y.; Du, Y. X.; Chen, G. X.; Qu, Y.; Jiang, J.; Zhu, Y. W. Strong light–matter interactions in sub-nanometer gaps defined by monolayer graphene: Toward highly sensitive SERS substrates. *Nanoscale* **2014**, *6*, 11112–11120.
[49] Duan, B.; Zhou, J. J.; Fang, Z.; Wang, C. X.; Wang, X. J.; Hemond, H. F.; Chan-Park, M. B.; Duan, H. W. Surface enhanced Raman scattering by graphene-nanosheet-gapped plasmonic nanoparticle arrays for multiplexed DNA detection. *Nanoscale* **2015**, *7*, 12606–12613.
[50] Le Ru, E. C.; Etchegoin, P. G. *Principles of Surface-Enhanced Raman Spectroscopy: And Related Plasmonic Effects*; Elsevier: Oxford, 2009.
[51] Liu, L.; Shao, M. W.; Cheng, L.; Zhuo, S. J.; Que, R. H.; Lee, S. T. Edge-enhanced Raman scattering effect from Au deposited nanoedge array. *Appl. Phys. Lett.* **2011**, *98*, 073114.
[52] Kudelski, A.; Pettinger, B. Fluctuations of surface-enhanced Raman spectra of CO adsorbed on gold substrates. *Chem. Phys. Lett.* **2004**, *383*, 76–79.
[53] Li, C. H.; Zhang, C.; Xu, S. C.; Huo, Y. Y.; Jiang, S. Z.; Yang, C.; Li, Z.; Zhao, X. F.; Zhang, S. Z.; Man, B. Y. Experimental and theoretical investigation for a hierarchical SERS activated platform with 3D dense hot spots. *Sens. Actuators B: Chem.* **2018**, *263*, 408–416.
[54] Li, X. H.; Choy, W. C. H.; Ren, X. G.; Zhang, D.; Lu, H. F. Highly intensified surface enhanced Raman scattering by using monolayer graphene as the nanospacer of metal film–metal nanoparticle coupling system. *Adv. Funct. Mater.* **2014**, *24*, 3114–3122.
[55] Lee, K. J.; Kim, D.; Jang, B. C.; Kim, D. J.; Park, H.; Jung, D. Y.; Hong, W.; Kim, T. K.; Choi, Y. K.; Choi, S. Y. Multilayer graphene with a rippled structure as a spacer for improving plasmonic coupling. *Adv. Funct. Mater.* **2016**, *26*, 5093–5101.
[56] Cançado, L. G.; Jorio, A.; Pimenta, M. Measuring the absolute Raman cross section of nanographites as a function of laser energy and crystallite size. *Phys. Rev. B* **2007**, *76*, 064304.
[57] Lee, J.; Shim, S.; Kim, B.; Shin, H. S. Surface-enhanced Raman scattering of single- and few-layer graphene by the deposition of gold nanoparticles. *Chemistry* **2011**, *17*, 2381–2387.
[58] Cancado, L. G.; Jorio, A.; Ferreira, E. H. M.; Stavale, F.; Achete, C. A.; Capaz, R. B.; Moutinho, M. V.; Lombardo, A.; Kulmala, T. S.; Ferrari, A. C. Quantifying defects in graphene via Raman spectroscopy at different excitation energies. *Nano Lett.* **2011**, *11*, 3190–3196.
[59] Das, A.; Chakraborty, B.; Sood, A. K. Raman spectroscopy of graphene on different substrates and influence of defects. *Bull. Mater. Sci.* **2008**, *31*, 579–584.
[60] Hildebrandt, P.; Stockburger, M. Surface enhanced resonance Raman study on fluorescein dyes. *J. Raman Spectrosc.* **1986**, *17*, 55–58.
[61] Wang, L. L.; Roitberg, A.; Meuse, C.; Gaigalas, A. K. Raman and FTIR spectroscopies of fluorescein in solutions. *Spectroch. Acta Part A: Mol. Biomol. Spectrosc.* **2001**, *57*, 1781–1791.
[62] Zhang, D. M.; Vangala, K.; Jiang, D. P.; Zou, S. G.; Pechan, T. Drop coating deposition Raman spectroscopy of fluorescein isothiocyanate labeled protein. *Appl. Spectrosc.* **2010**, *64*, 1078–1085.
[63] Dou, X.; Chung, P. Y.; Jiang, P.; Dai, J. L. Surface plasmon resonance and surface-enhanced Raman scattering sensing enabled by digital versatile discs. *Appl. Phys. Lett.* **2012**, *100*, 041116.
[64] Maurer, T.; Nicolas, R.; Lévêque, G.; Subramanian, P.; Proust, J.; Béal, J.; Schuermans, S.; Vilcot, J. P.; Herro, Z.; Kazan, M. et al. Enhancing LSPR sensitivity of Au gratings through graphene coupling to Au film. *Plasmonics* **2014**, *9*, 507–512.
[65] Zhu, J. F.; Liu, Q. H.; Lin, T. Manipulating light absorption of graphene using plasmonic nanoparticles. *Nanoscale* **2013**, *5*, 7785–7789.
[66] Wang, D. Q.; Bourgeois, M. R.; Lee, W. K.; Li, R.; Trivedi, D.; Knudson, M. P.; Wang, W. J.; Schatz, G. C.; Odom, T. W. Stretchable nanolasing from hybrid quadrupole plasmons. *Nano Lett.* **2018**, *18*, 4549–4555.